Available online at www.sciencedirect.com

SCIENCE DIRECT®

Coastal Engineering 52 (2005) 285–302

Coastal Engineering
An International Journal for Coastal, Harbour and Offshore Engineers

www.elsevier.com/locate/coastaleng

Prediction of swash motion and run-up including the effects of swash interaction

Li Erikson*, Magnus Larson, Hans Hanson

Department of Water Resources Engineering, Lund University, Box 188, 221 00, Lund, Sweden

Received 5 February 2004; received in revised form 4 May 2004; accepted 14 December 2004

Abstract

Modifications to a model describing swash motion based on solutions to the non-linear shallow water equations were made to account for interaction between up-rush and back-wash at the still water shoreline and within the swash zone. Inputs to the model are wave heights and arrival times at the still water shoreline. The model was tested against wave groups representing idealized vessel-generated wave trains run in a small wave tank experiment. Accounting for swash interaction markedly improved results with respect to the maximum run-up length for cases with rather gentle foreshore slopes ($\tan\beta$=0.07). For the case with a steep foreshore slope ($\tan\beta$=0.20) there was very little improvement compared to model results if swash interaction was not accounted for. In addition, an equation was developed to predict the onset and degree of swash interaction including the effects of bed friction.

Keywords: Run-up; Swash; Wave groups; Vessel-generated waves; Ballistic model

1. Introduction

Modeling of the hydrodynamics in the swash zone has seen many advances in recent years. It is now fairly well established that swash motion is driven by low frequency infra-gravity motions and bores which collapse at the shoreline and then propagate up the beach face. The two mechanisms do not appear to be exclusive, but rather, one dominates over the other depending on the incident waves and foreshore slope. There have also been several observations and attempts to describe interaction between subsequent swash waves within the swash zone. Holland and Puleo (2001) recently showed that the presence or lack of swash collisions might describe whether foreshores accrete or erode (this was also suggested by Kemp, 1975). On foreshore slopes where swash excursion times are of longer duration than the incident wave period, steepening is expected to occur. In contrast, on beaches where the swash is of shorter duration than the incoming bores, erosion is expected to occur and the foreshore will be flattened.

* Corresponding author. Tel.: +1 831 476 8582.
E-mail address: li.erikson@sbcglobal.net (L. Erikson).

0378-3839/$ - see front matter © 2005 Elsevier B.V. All rights reserved.
doi:10.1016/j.coastaleng.2004.12.001

The impetus for this study was to gain some insight into swash behavior due to waves generated by moving vessels although it is believed that the results are applicable to a wider range of wave conditions. A moving ship typically generates a set of waves at both its bow and stern as a consequence of pressure gradients along the hull. These waves are often referred to as wash waves and, when measured some distance from the navigation route of a vessel they consist of a group of waves that increase in height to some maximum and subsequently decrease. When these waves reach the shore there is often significant interaction between subsequent waves such that when a wave reaches the shoreline and travels up a beach face it is not always able to complete a full swash cycle before the next wave comes along. This second wave either overtakes the first wave during its up-rush stage (catch-up) or collides with the first wave during the back-wash stage. This interaction between waves continues with each incoming wave, and with respect to the hydrodynamics, the end result is that the maximum run-up will not correspond to the up-rush of the highest wave in the train. This is particularly true for mild foreshore slopes ($\tan\beta<0.1$) where the time it takes for a swash lens to travel up and down is longer than for steeper slopes (Mase and Iwagaki, 1984).

The objective of this study was to develop a simple physically-based approach to describe the shoreline motion while accounting for interaction between subsequent waves in the swash zone. A particular focus on vessel generated waves was also the intent. A description of the shoreline motion due to collapsing bores at the still water shoreline is particularly suitable for modeling swash interaction and, thus, this already well established approach was modified to incorporate swash interaction. An equation describing the onset of swash interaction, including the effects of friction is derived. The equation is tested and numerical results of the model with and without swash interaction for data from a laboratory experiment conducted in part for this study are presented.

2. Literature review

The hypothesis that the time-varying position of the leading edge of the shoreline can be described by collapsed bores that move up and down a slope as a mass of water was first described by Ho et al. (1963) and Shen and Meyer (1963). They derived a set of governing equations, based on the non-linear shallow water equations (NLSWE) together with mathematical and physical interpretations of singularities at the point of bore collapse and maximum run-up. Waddell's (1973) field observations supported the hypothesis. He noted that during the up-rush, and initial stages of the back-wash, the leading edge behaved like a unit mass moving up and down the foreshore under the action of gravity, neglecting friction.

Hughes (1992) applied the non-linear shallow water theory to field data from a number of natural sandy beaches with steep foreshore slopes ($\tan\beta=0.093$ to 0.15). A comparison between measurements and inviscid theory replicated the gross flow behavior of the up-rush well, but overestimated the maximum run-up by as much as 65%. He speculated that the difference in magnitude was due to not accounting for bed friction and infiltration (median grain size diameters of $D_{50}=0.31$ mm to $D_{50}=2.00$ mm). Hughes (1995) added a stress term for bed friction to the non-linear shallow water theory and solved the equations with measured values to obtain an inferred friction value of 0.1 for the up-rush. Similarly, Holland and Puleo (2001) obtained estimates of up-rush and back-wash friction factors by iterating on f using the non-linear shallow water theory (also termed 'ballistic model') and compared the results to measured data obtained at Duck in 1994 ($D_{50}=0.22$ mm). Analysis of over 2000 individual swash events showed that an up-rush friction coefficient of $f_u=0.01$ and back-wash friction coefficient $f_b=0.04$ gave the best results with respect to the minimum overall error between calculated and measured swash trajectories. The authors also noted that during the field campaign, the foreshore slope decreased from about 0.19 to 0.06 and that the foreshore seemed to adjust in order to minimize swash interaction. By iterating on f, they essentially accounted for swash interaction by adjusting the friction terms.

The catch-up and absorption mechanism of swash interaction was explicitly modeled by Mase and Iwagaki (1984) employing empirical data and

Mase (1988) and Baldock and Holmes (1999) by superimposing run-up parabolas using the ballistic model without friction. Mase and Iwagaki (1984) ran a series of tests in the laboratory with random waves and found that the ratio of the number of individual run-up waves to that of incident waves decreased as the beach slope decreased. Based on additional laboratory experiments, Mase (1989) developed an empirical formula to predict the maximum run-up on a range of slopes while accounting for swash interaction between random waves. Baldock and Holmes (1999) presented experimental data and found excellent agreement between predicted values and measured swash motion for regular waves, wave groups, and random waves on a steep (1:10) impermeable beach in a laboratory setting. Although the experiment was conducted on a fairly steep beach face, they reported considerable interaction between subsequent bores in the swash zone, for the cases where bi-chromatic wave groups of varying height were run. The interaction often caused the smallest bores at the beginning of the group to run up further than the subsequent larger bores.

It appears that the collision mechanism of swash interaction has not previously been explicitly accounted for in the ballistic model. An overview of the model and modifications done for this study are presented in the following section and simulation results with and without the collision mechanism are presented in Section 5.

3. Model formulation

3.1. Model basis

The model is based on the hypothesis that swash motion is largely driven by bores that collapse at the shoreline and then propagate up the beach face (Ho et al., 1963; Shen and Meyer, 1963; Hibberd and Peregrine, 1979). By considering a fluid element at the leading edge of a collapsed bore (swash lens), a force balance can be derived (Kirkgöz, 1981; Hughes, 1995; Puleo and Holland, 2001):

$$\frac{\mathrm{d}^2 x_s}{\mathrm{d}t^2} = -g\sin(\beta) \pm \frac{f}{2\delta h}\left(\frac{\mathrm{d}x_s}{\mathrm{d}t}\right)^2 \quad (1)$$

where the coordinate system has x positive onshore (along the foreshore) and z positive upwards, t=time, x_s=shoreline position of the swash front relative to the initial shoreline position (Fig. 1), g=acceleration due to gravity, β=beach slope angle, f=friction factor, and δh=height of the leading fluid element. If g, β, f and δh are constant, then Eq. (1) can be integrated using separation of variables to yield the

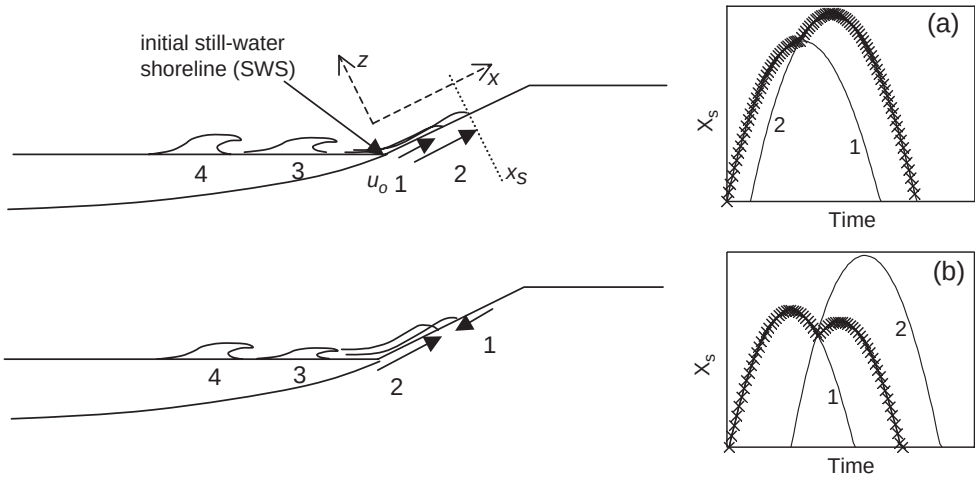

Fig. 1. Sketch illustrating two phenomena accounted for in the swash interaction model. (a) Catch-up and absorption, and (b) up-rush and back-wash collision.

up-rush, u_{su}, and back-wash, u_{sb}, shoreline (swash front) velocities,

$$u_{su}(t) = \frac{dx_s}{dt} = \sqrt{\frac{2g\delta h_u \sin(\beta)}{f}}\tan(F+G)$$

$$u_{sb}(t) = \frac{dx_s}{dt} = -\sqrt{\frac{2g\delta h_b \sin(\beta)}{f}}\tanh(E) \quad (2)$$

where u_{su} (t=0)=u_0, u_0=initial shoreline velocity, t=0 when the swash front is at the initial shoreline position or still water shoreline, SWS, and u_{sb} (t=0)=0 with the swash front at the maximum landward position. Surprisingly, the time-dependent back-wash equation does not appear to have been published previously. The initial shoreline velocity, u_0, is assumed to occur at the SWS, and is estimated with (Svendsen and Madsen, 1984),

$$u_0 = C\sqrt{gH} \quad (3)$$

where H is the wave height, taken at the SWS, and C is an empirical coefficient describing the resistance. Theoretically, C ranges from 1 to a maximum of 2 for no bed resistance, whereas a typical value for a dry sand bed is C=1.83 (Cross, 1967; Miller, 1968; Yeh et al., 1989). A value of 1.83 for C was used for all simulations in this study.

The sign in Eq. (1) indicates the direction of the velocity (positive for up-rush and negative for back-wash) and the terms E, F, and G are given by,

$$E = \frac{1}{2}t\sqrt{\frac{2gf\sin(\beta)}{\delta h}}$$

$$F = -t\sqrt{\frac{gf\sin(\beta)}{2\delta h}}$$

$$G = \tan^{-1}\left[\frac{u_0\sqrt{f}}{\sqrt{2g\delta h\sin(\beta)}}\right] \quad (4)$$

where δh takes on the value of δh_u or δh_b depending on direction and with t=0 at the start of each swash phase. Integrating Eq. (2) with respect to t using the boundary condition that the shoreline displacement is zero (x_s=0) at t=0 for the up-rush and x_s is equal to the run-up length at t=0 for the back-wash, yields the time–space history of the leading edge of the swash front (Hughes, 1995; Puleo and Holland, 2001):

$$x_{su}(t) = \frac{2\delta h_u}{f_u}\ln\left(\frac{\cos(F+G)}{\cos(G)}\right)$$

$$x_{sb}(t) = -\frac{2\delta h_b}{f_b}\ln(\cosh(F)) \quad (5)$$

The maximum run-up height, z_m, can be found by manipulation of Eqs. (2) and (5) and trigonometry:

$$z_m = \frac{-2\delta h_u \sin\beta}{f_u \tan\beta}\ln\cos(G) \quad (6)$$

Eq. (5) describes a parabolic motion skewed by the friction factors. Following Puleo and Holland (2001) and as suggested by Hughes (1995), two different formulations are used to calculate the friction factors,

$$f = \frac{2}{\left(2.5\ln\left[\frac{10\delta h}{D_{90}}\right]\right)^2} \quad (7)$$

and

$$f = \frac{2}{\left(2.5\ln\left(\frac{5.32\delta h\rho g(s-1)}{\tau}\right)\right)^2} \quad (8)$$

where D_{90}=90th percentile on the cumulative grain size curve, s=ratio of sediment to water density, ρ=fluid density, and τ=shear stress term related to bed roughness (τ=1/2$\rho f|u_s|u_s$).

Eq. (7) is commonly referred to as the 'Law of the Wall' and Eq. (8) is a sediment-laden sheet flow formulation (e.g., Van Rijn, 1982; Wilson, 1988; Hughes, 1995). The former equation is used when a clear-fluid flow without much sediment transport is predicted, whereas Eq. (8) is used to describe flow resistance with significant sediment transport. In both cases δh takes on either δh_u or δh_b depending on the flow direction. Wilson (1989) showed that sheet flow conditions (Eq. (8)) predominate when the value of the Shield's parameter, Θ, is greater than 0.8 where Θ is defined as,

$$\Theta = \frac{\tau}{\rho g D_{50}(s-1)} \quad (9)$$

where D_{50}=median grain size diameter. The shear stress term in the numerator is calculated using Eq. (7)

with the mean up-rush or back-wash velocity from Eq. (2). For swash conditions where $\Theta<0.8$, the "Law of the Wall" friction factor, Eq. (7), is used and for conditions where $\Theta\geq0.8$, the sediment-laden friction factor, Eq. (8), is solved iteratively. An iterative approach is necessary due to the shear stress term in the denominator which is a function of f as well. The approach is somewhat computationally inefficient in that the swash front velocities are first calculated using a clear-fluid formulation for the friction factor, and if it is found that the value of the Shield's parameter, itself a function of the friction factor, exceeds 0.8, the swash front velocities and time trajectories are recalculated using the sediment-laden friction factor. This approach is used in this model to allow for a theoretical estimate of the friction term, f, as opposed to using an empirical value. The method allows for different up-rush and back-wash friction values (e.g., $f_u\neq f_b$), but requires that they are constant during the swash phase in question.

3.2. Swash interaction

The model accounts for two processes in the interaction between successive bores within the swash zone above the SWS. The first is 'catch-up and absorption' where the front of a wave moving landward (up-rush) is passed by a subsequent bore moving in the same direction (Fig. 1a). The model simulates the position and velocity of the leading edge of the swash (i.e., Eqs. (5) and (2)), and so, in the case of catch-up and absorption, the model is written to follow the faster swash front, effectively drowning the first but slower up-rush. The second process is 'collision' whereby two separate fronts collide as the back-wash of a preceding swash lens meets the front of a subsequent swash wave during its up-rush phase as depicted in Fig. 1b. For such a case, a new leading edge velocity is calculated based on the principals of momentum.

The momentum (mass times velocity) is calculated for both the up-rush and back-wash at the point (and time) where the fronts meet. To calculate the momentum it is assumed that a fluid element of length l_s at the leading edge of the up-rush collides with a fluid element of the same length, at the leading edge of the back-wash. The mass of each are $m_u=\delta h_u l_s \rho$ and $m_b=\delta h_b l_s \rho$, and the momentums are $M_u=m_u u_{su}(t)$ and $M_b=m_b u_{sb}(t)$, for the up-rush and back-wash, respectively. A new velocity following collision, u_s^{coll}, is determined from the average of the up-rush and back-wash momentums and assuming that momentum is conserved,

$$u_x^{coll}=\frac{M^{coll}}{m_b}\ \text{for}\ M^{coll}>0$$

$$u_x^{coll}=\frac{M^{coll}}{m_u}\ \text{for}\ M^{coll}<0 \tag{10}$$

where

$$M^{coll}=\frac{M_u+M_b}{2}. \tag{11}$$

For the formulation presented here, $m_b<m_u$ (see Section 5.2) and hence the conditions of negative or positive values of M^{coll} in Eq. (10) were set.

The new velocity after collision (Eq. (10)) may be negative and hence the u-subscript is not specified on u_s^{coll}. A negative value would indicate that the up-rush is fully drowned by the returning back-wash.

Swash interaction at the SWS is explicitly accounted for in the model by imposing an exponentially decreasing velocity of the returning back-wash at the SWS. Velocities calculated with Eq. (2) go to zero after the swash front passes the SWS causing a discontinuity in the model as the back-wash 'disappears' at this point. If the velocity is allowed to go to zero at the SWS, initial shoreline velocities may be overestimated since they are not measured directly but are calculated with measured wave heights at the SWS (Eq. (3)); any retarding effect that the back-wash may have on the initial up-rush velocity will not be included if the back-wash is allowed to go to zero at the SWS. The decreasing velocity at the SWS immediately after the waves pass is described by $u(t)=u_{sws}e^{-\alpha t}$, where $t=0$ as the swash front passes the SWS, u_{sws} is the velocity at the SWS at $t=0$, $\alpha=\sin(\beta)/h_s$ and h_s is the water depth at the boundary of the surf and swash zones (arbitrarily set at 0.03 m for these simulations).

3.3. Potential for swash interaction

The potential for interaction between subsequent swash waves on the beach above the SWS may be

estimated by comparing the duration of a complete swash cycle with the period of the incident waves. If the duration of the swash cycle exceeds the incident wave period, then interaction is expected. Because friction has been introduced to describe the swash front's position, the predicted motion is asymmetric and the time for the up-rush to reach the maximum point of landward displacement, T_{su}, is shorter than the time required for the back-wash to return to the SWS, T_{sb}. The duration of the up-rush can be derived by noting that $u_{su}=0$ at the time of maximum landward retreat (setting $u_{su}=0$ in Eq. (2)); the duration of the back-wash can be obtained by setting the travel distance of the back-wash equal to the up-rush ($x_{sb}=x_{su}$). The total swash duration is given by $T_s=T_{sb}+T_{su}$,

$$T_s = \frac{\ln\left(A+\sqrt{A^2-1}\right)u_0}{g\tan(G_b)\sin(\beta)} + \frac{G_u u_0}{g\tan(G_u)\sin(\beta)} \qquad (12)$$

where $A=1/\cos(G_b)$, and the b and u subscripts of G refer to values for back-wash and up-rush, respectively. If $f_b=f_u=f$ and $\delta h_b=\delta h_u=\delta h$, then the effects of friction can be assessed by dividing Eq. (12) by the total swash duration neglecting friction ($T_{sg}=(2u_0)/(g\sin\beta)$) so that,

$$\frac{T_s}{T_{sg}} = \frac{1}{2\sqrt{\varepsilon}}\left(\arctan\left(\sqrt{\varepsilon}\right)+\ln\left(A_\varepsilon+\sqrt{A_\varepsilon^2-1}\right)\right) \qquad (13)$$

where $A_\varepsilon=1/\cos(\arctan(\sqrt{\varepsilon}))$ and $\varepsilon=fu_0^2/2\delta hg\sin(\beta)$. The parameter ε expresses the ratio between friction and gravity. At the limit where ε approaches zero, the right-hand side of Eq. (13) becomes 1. Fig. 2 plots T_s/T_{sg} as a function of ε, as well as T_{su}/T_{sg} and T_{sb}/T_{sg}. The figure shows that the swash duration is always shorter if friction is included, and that the duration of the back-wash is always longer than the up-rush.

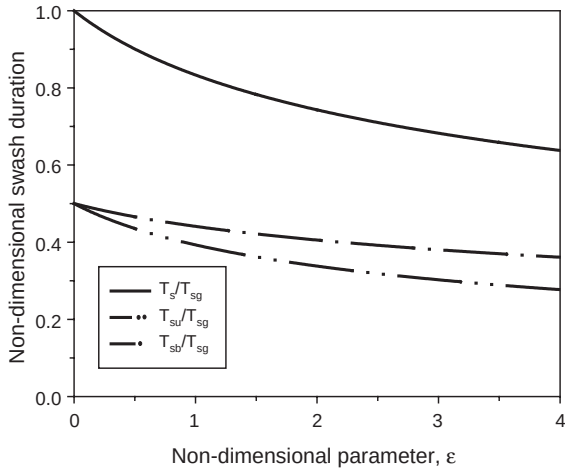

Fig. 2. The effects of friction on swash duration. T_{su}, T_{sb}, T_s are calculated swash durations, including friction, of the up-rush, back-wash and full cycle, respectively. T_{sg} is the calculated swash duration without friction.

4. Experimental setup

4.1. Wave flume

A 27-m section of a wave tank at the Engineering Research and Development Center, U.S. Army Corps of Engineers in Vicksburg, Mississippi was used for the experiment. The tank measured 0.91 m in width, and 0.91 m at maximum depth. Waves were generated by a horizontally displacing piston-type paddle in a water depth of at least 0.5 m. The experimental setup is shown in Fig. 3.

Uniform sand with a median grain size diameter (D_{50}) of 0.13 mm and a fall speed of 1.4 cm/s was used in the experiment. The beach profile beneath the still water line was graded to represent an equilibrium profile. Foreshore slopes above the initial still water line were $\tan\beta=0.20$ (1:5, vertical to horizontal) or $\tan\beta=0.07$ (1:15), depending on the case.

4.2. Instrumentation

A total of 14 standard capacitance gauges were used in the experiment, 3 of which were at or landward of the SWS. The gauges are estimated to measure with an accuracy of 0.5%. Two digital video cameras (Sony, models PC100E and TRV6E) were used to record the vertical elevation of the water surface at the SWS and the run-up lengths. The cameras were of the PAL (Phase Alternative System) Western European and Australian standard

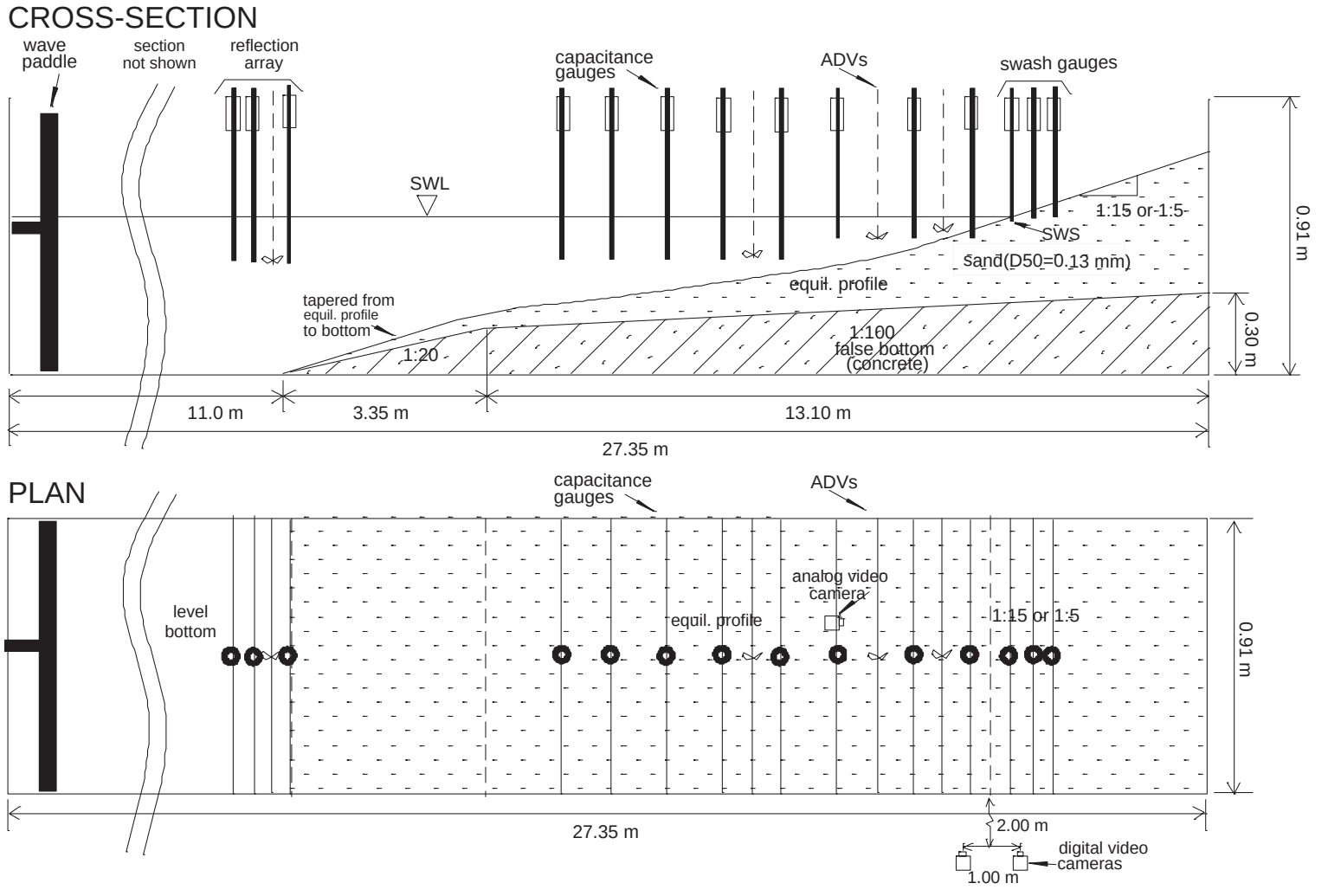

Fig. 3. Laboratory set-up of the experiment. A cross-section of the tank is shown in the upper plot and a plan view is shown in the lower plot.

with a captured image resolution of 720 by 576 pixels at 25 frames per second. The sampling frequency of the capacitance wave gauges was also set to 25 Hz to match the cameras. The cameras were mounted on standard tripods and positioned approximately 2 m from the sidewall of the tank so that nominal pixel resolution was better than 2 mm with a horizontal field of view (FOV) of less than 1.5 m for each camera. Accurate time synchronization between the cameras and the gauge logger was not possible due to logistical difficulties. However, a digital clock was displayed in the common camera FOV to assist in image synchronization. The water was dyed fluorescent green to improve image contrast, and a grid of control points was marked on the outside of the glass tank wall (target plane) with an origin defined at the SWS to allow post-processing rectification. A more detailed description of the methodology can be found in Erikson and Hanson (2005).

4.3. Wave generation

The study presented herein considers idealized wave packets representing waves generated by typical conventional and high-speed large ferries. Based on a review of the literature, supplemented with field measurements, and Airy wave theory, wave trains where the wave height increases to some maximum and consequently decreases are thought to be simplified first-order representations of secondary waves generated by moving vessels. As an example, wave trains measured in the field in deep water following the passage of two vessels are shown in

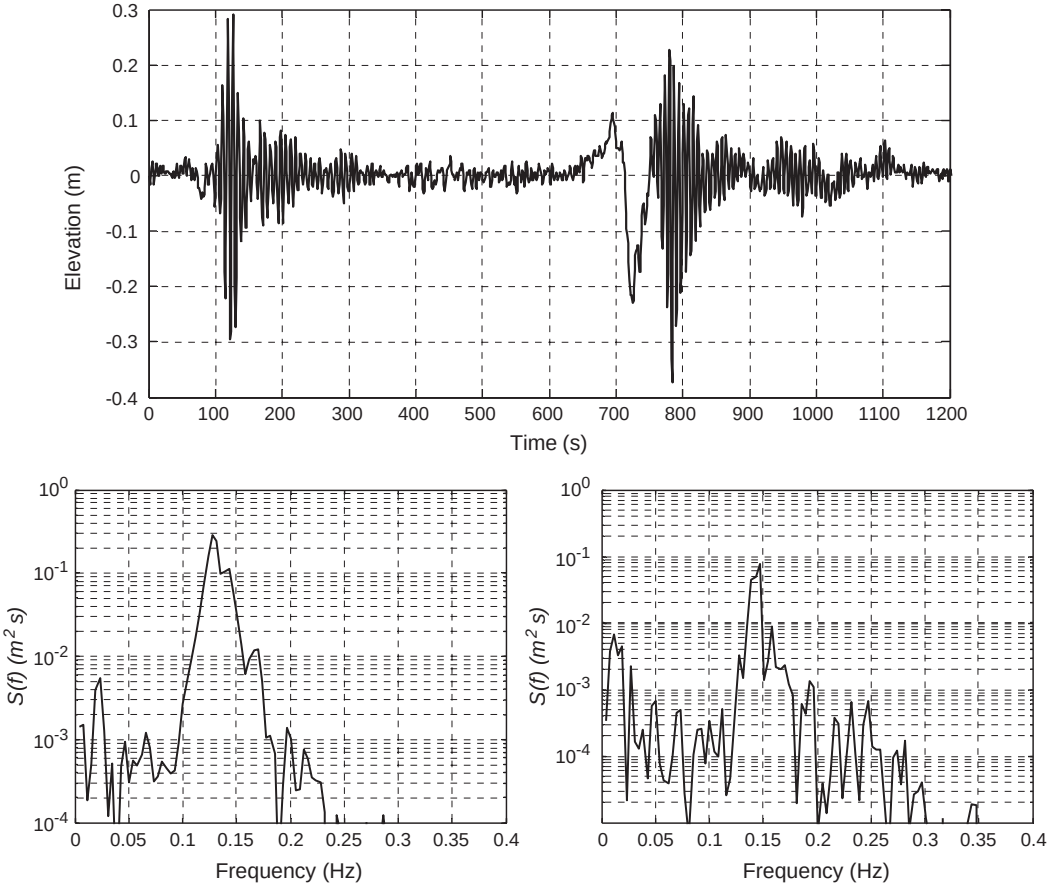

Fig. 4. Surface elevations following the passage of two large passenger carrying vessels and the associated energy spectrums.

Table 1
Summary of experimental conditions

Case	T (s)	f_m (Hz)	H_0 (m)	H_0/L_0	Foreshore slope (tanβ)	Surf similarity, ξ
C1	1.7	0.06	0.18	0.040	0.20	0.13–0.80
B8	1.3	0.08	0.13	0.049	0.07	0.17–0.99
B9	1.3	0.08	0.18	0.068	0.07	0.11–1.08
B10	2.2	0.05	0.13	0.017	0.07	0.30–1.63

Fig. 4 (Johansson, 2000). The first wave packet from about 50 to 300 s was generated by a high-speed vessel while the surface elevations from about 650 s onward are from a conventional displacement vessel. The initial decline of the water surface (from 700 s to 750 s) is due to the displacement of the ship and is not considered in this study. Note however that the shorter waves of both wave trains are quite similar in that they increase in height and subsequently decrease. This is quite typical and can be readily seen or extracted when specified energy components are filtered out. The power spectrums of each are shown in the lower plots of the figure and indicate that for the first wave train, the majority of the energy is concentrated around 0.13 Hz. For the second wave train, most of the energy is concentrated around 0.15 Hz but there is also significant energy in the lower and greater frequencies up to about 0.25 Hz. Based on similar analyses of several wave trains and a comprehensive literature review it seems that the majority of significant energy for typical vessel generated wave trains lies below 0.25 Hz (i.e., greater than 4 s).

The idealized wave packets employed in the experiment consisted of wave trains with increasing and subsequently decreasing wave heights and individual wave periods from 4.1 s to 7 s. The upper limit was set to avoid spurious wave generation in the small wave tank. A time-scale factor of 1:3.16 (corresponding to a length-scale factor of

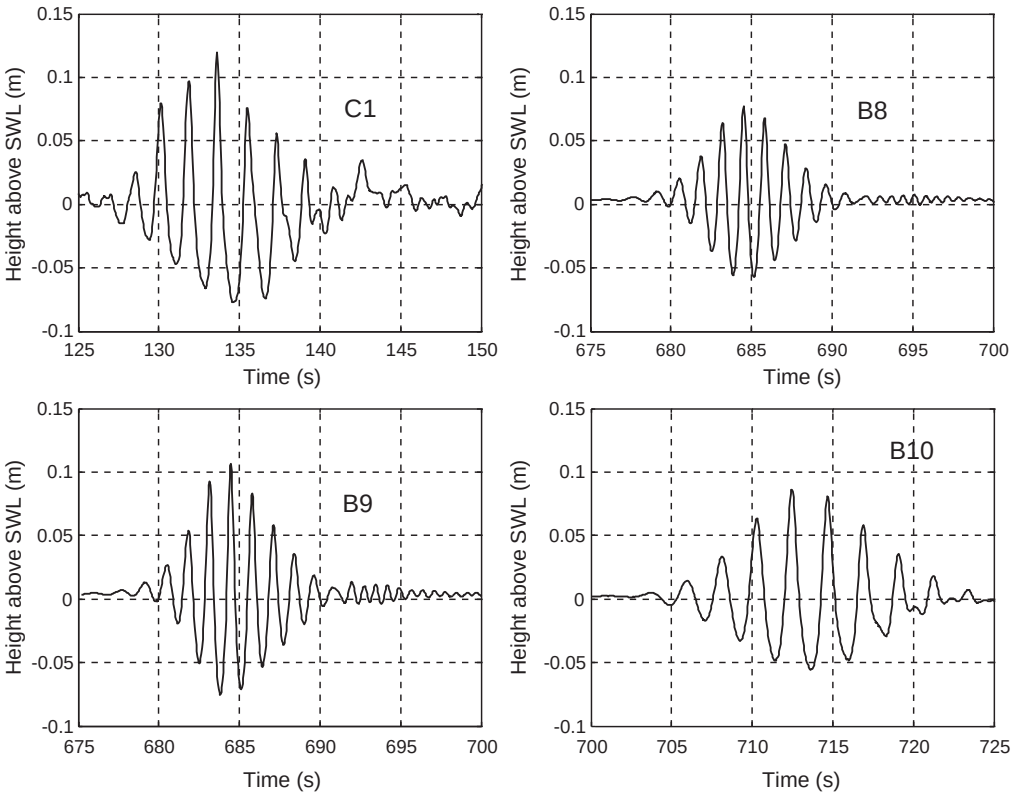

Fig. 5. Offshore wave trains measured approximately 14 m from SWS.

1:10) was employed so that the chosen periods run in the laboratory were 1.3 s, 1.7 s, and 2.2 s (prototype 4.1 s, 5.4 s, and 7 s). A summary of the wave conditions is listed in Table 1. The wave heights were set intentionally high in order to obtain well quantifiable results in the laboratory and model extreme cases. The fourth column in Table 1 lists the maximum wave height near the paddle in each group and for each case. The greatest wave steepness (H_0/L_0) is listed in column 5. The value of the surf similarity parameter, $\xi = \varphi/\sqrt{H_0/L_0}$ (where φ is the surf zone slope near the break point (Irribarren and Nogales, 1949)) varied for each wave within a given wave train suggesting a combination of spilling and plunging waves in the surf zone.

The generated wave trains were constructed by multiplying sinusoidal waves of the chosen individual wave periods with a second sinusoidal wave modulated at the group frequency (f_m, listed in column 3 of Table 1) such that each wave packet consisted of 10 waves. Offshore surface elevations measured at the most seaward gauge (about 14 m from the SWS) are shown in Fig. 5 for the four cases presented in this paper. Water depths at the paddle were 0.56 for the B cases and 0.50 for case C1. The slightly more shallow water depth of case C1 in conjunction with the longer wave period 2.2 s caused the waves to shoal slightly at the offshore location.

Although more than a total of 100 wave trains were run, results of only one wave train from each case are presented here. The wave motion was highly repeatable and although the beach consisted of movable sand, little sediment transport was obtained so that results between subsequent bores only differed slightly. Wave trains were generated with a half a minute lag for case C1 and a 3.5 min lag for the remaining cases between subsequent groups. This was done to minimize wave reflection in the tank and to simulate the passage of one vessel at a time. Analysis of the wave records was done on sampled intervals spanning only the time of significant run-up and less than the time required for waves to reflect off the beach and paddle and return to the SWS. This procedure eliminated contamination of the data by waves reflected off the board, but included the natural reflection of waves by the beach.

5. Results

5.1. Measured run-up and swash depth

Fig. 6 shows time series of measured run-up lengths, plotted against the left axis, and swash depths measured at the SWS, plotted against the right axis, for the selected wave trains. Note that on this and similar figures the run-up is plotted in terms of run-up length, rather than run-up height (as was done by e.g., Baldock et al., 1997). This is to emphasize the two different reference frames within which the measurements were made. The run-up data were obtained in a Lagrangian reference frame (following the swash front motion) while the swash depth was obtained at the initial SWS in an Eulerian reference frame (i.e., fixed).

For the cases with $\tan\beta$=0.07, the duration of the wave packets measured at the SWS decreased by about 23% to 35% (from about 13 to 20 s measured offshore to 10 to 13 s measured at the SWS). For all four cases, the number of discernable peaks reduced from 10 to between 5 and 7. The "disappearing" waves appear to be a consequence of returning backwash either colliding with incoming bores seaward of the SWS or absorbing the incident bores at the SWS.

A spectral analysis of the swash depth at the SWS was performed with a fast Fourier transform (FFT) using the Welch method and 1024 data points sampled at 25 Hz. The results are shown in Fig. 7 and indicate that although there is considerably high energy at the lower frequencies, much short wave energy is still present. The presence of short wave energy at the SWS supports the notion of using the bore collapse model, as opposed to a low-frequency standing wave model (Section 1), to describe the run-up or shoreline motion. The presence of the long wave energy (at the low frequencies) is probably related to the up-rush/back-wash interaction in the swash zone (Mase, 1994) and likely describes the envelope of the run-up reached by individual bores as shown by Baldock et al. (1997).

Looking back at Fig. 6 it is clear that the run-up (shoreline motion) is driven by the swash height at the SWS. Most of the peaks observed at the SWS are also observed in the shoreline motion. Cross-correlations between measured swash depth and run-up length are shown in Fig. 8 and suggest that there is a similar variation with time and that the variation of the swash

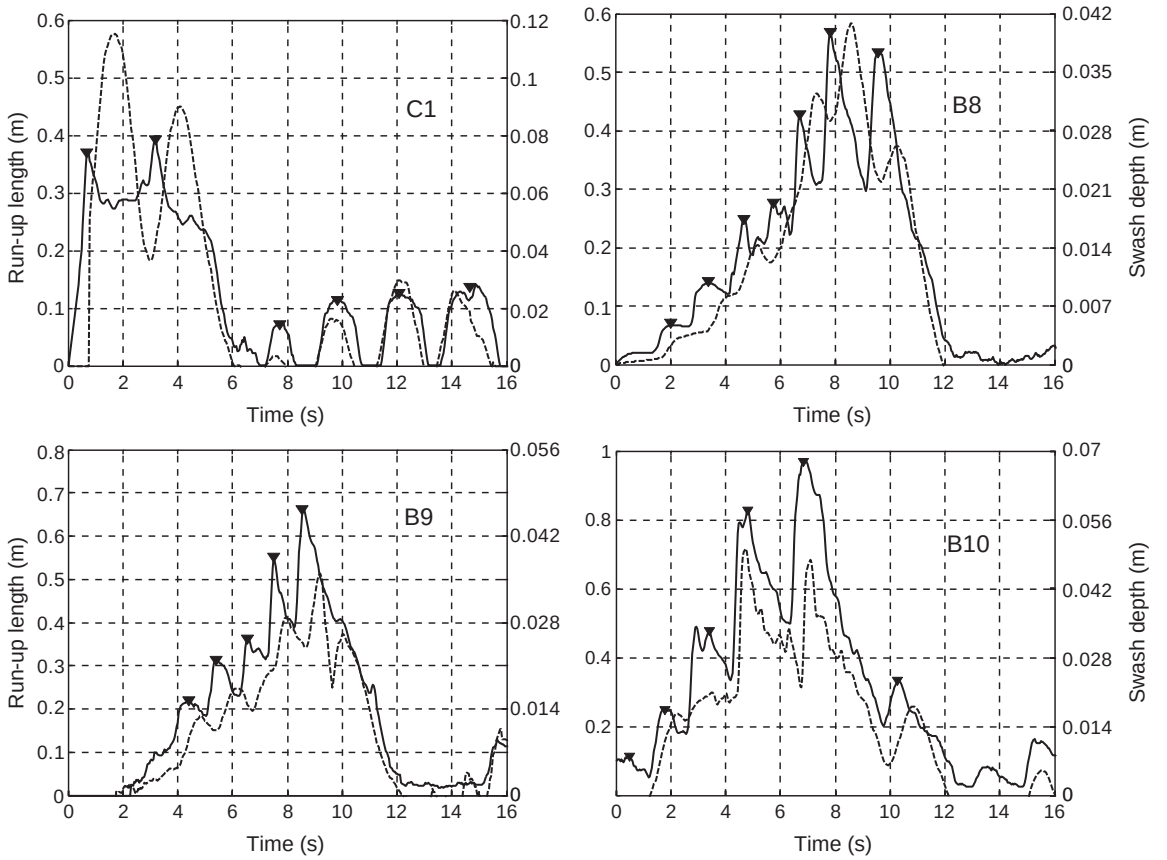

Fig. 6. Measured run-up lengths (dashed lines) and swash depths at the initial still water shoreline (solid lines). Bore heights and arrival times input to model are shown with downward pointing triangles. (N.B. Vertical scale differs between panels).

depth precedes the variation of the run-up. This is important as the measurements taken at the SWS contain some part of the run-up signal due to the backwater returning to the SWS. It is also apparent from the peaks of the curves, shown with the solid circles on the inset of the figure, that there is a phase shift of less than half a second between the run-up and swash depth at the SWS. Furthermore, there is a negative correlation between the phase shift and incident wave period so that the greater the incident wave period, the shorter the phase lag.

5.2. Modeled run-up

In Fig. 9, measured run-up lengths are compared to run-up lengths calculated with the model described in Section 3. Model results without accounting for swash interaction are shown in Fig. 10. Because the maximum run-up heights are substantially different for cases B8 through B10 depending on whether swash interaction is accounted for or not, the vertical scales in Figs. 9 and 10 are not consistent for a given case. If the vertical scales were the same, much detail between measured and calculated run-up lengths would not be visible in Fig. 9. Inputs to the model are bore heights and their arrival time at the SWS. The bore heights and arrival times at the SWS are taken at the peaks of the time series in Fig. 6 as depicted by the downward facing triangles. Up-rush leading edge heights (δh_u) were estimated by iteration of the empirical equation presented by Hughes (Eqs. (19) and (20), 1992):

$$\delta h_u = h_s^* z_m \tag{14}$$

where $h_s^*=0.21-0.48x_*+0.32x_*^2$ and x_* is the dimensionless distance from the initial shoreline position to

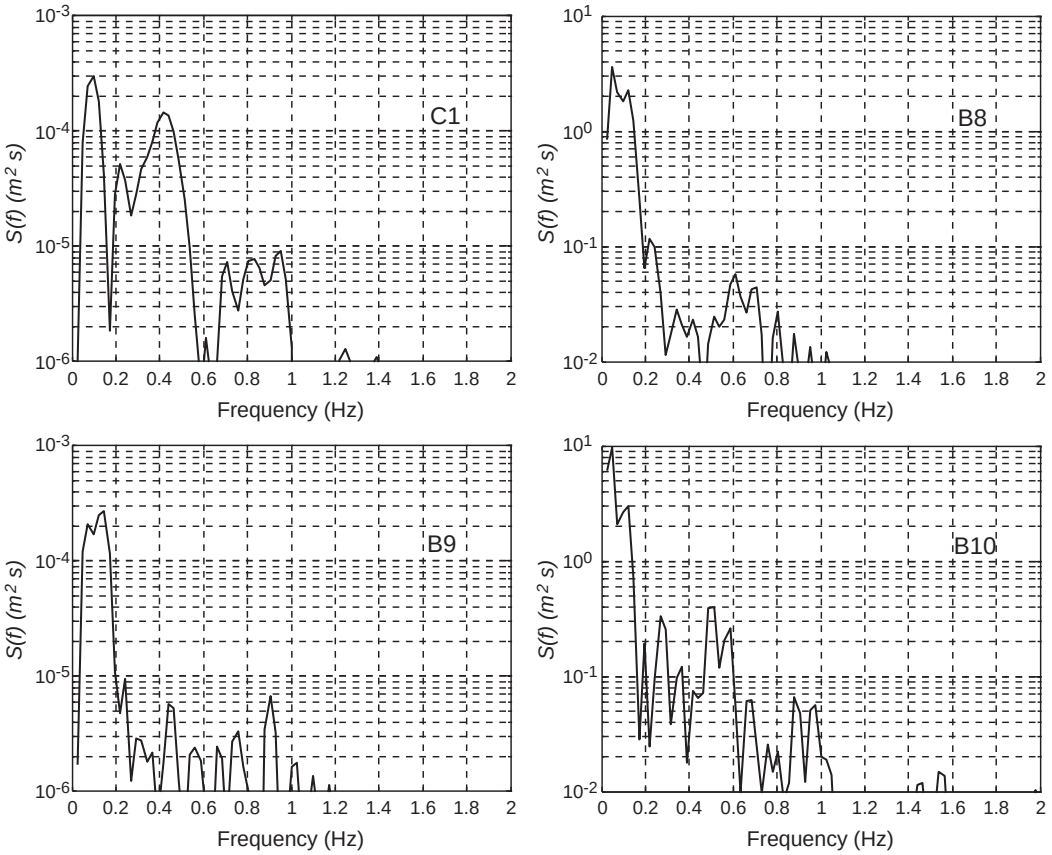

Fig. 7. Power spectra of swash depths measured at SWS. (N.B. Vertical scale differs between panels).

the maximum run-up length. The mid-swash position represented by x_*=0.5 was used in all simulations as suggested by Hughes (1995). The maximum run-up height, z_m, in Eq. (14) was calculated with Eq. (6) in combination with the friction factors by either Eq. (7) or (8). Mean values (for all waves of each case) were found to be δh_u=2 cm for cases C1 and B8 and δh_u=4 cm for cases B9 and B10. Measurements obtained from both video images and the most landward gauges (Fig. 1) indicate that δh_u was on the order of 2 cm to 3 cm. Discrepancies between measured and predicted values differ on a case-by-case basis, with the maximum difference less than 1.8 cm.

Hughes et al. (1997) reviewed several laboratory and field studies and found that the thickness of the up-rush, δh_u, was consistently greater than the back-wash height, δh_b. Based on Atlantic Coast field data, Holland and Puleo (2001) estimated that the back-wash height was 60% of the up-rush (δh_u=5 cm and δh_b=3). This ratio (δh_b=0.60δh_u) was employed in the model so that average leading edge back-wash heights were in the range of 1 to 2.4 cm. The results in Fig. 9 are with δh_b=0.6δh_u for all cases except B9 where δh_b=0.75δh_u. The greater relative back-rush height resulted in a decrease of the maximum run-up from 0.73 m to 0.48 m, which is significantly better compared to the measured run-up length of 0.49 m. For cases with significant swash interaction, the model is quite sensitive to changes of δh_b. To illustrate this point, maximum calculated run-up lengths normalized by measured maximum run-up lengths are plotted against $\delta h_b/\delta h_u$ in Fig. 11. The graph shows that the maximum run-up length is best estimated with $\delta h_b/\delta h_u$=0.60 for cases B8 and B10, while $\delta h_b/\delta h_u$=0.75 yields the best estimate for case B9. For case C1, where there is little swash interaction, any value of $\delta h_b/\delta h_u$>0.4 yields equally good results with respect to the maximum run-up length.

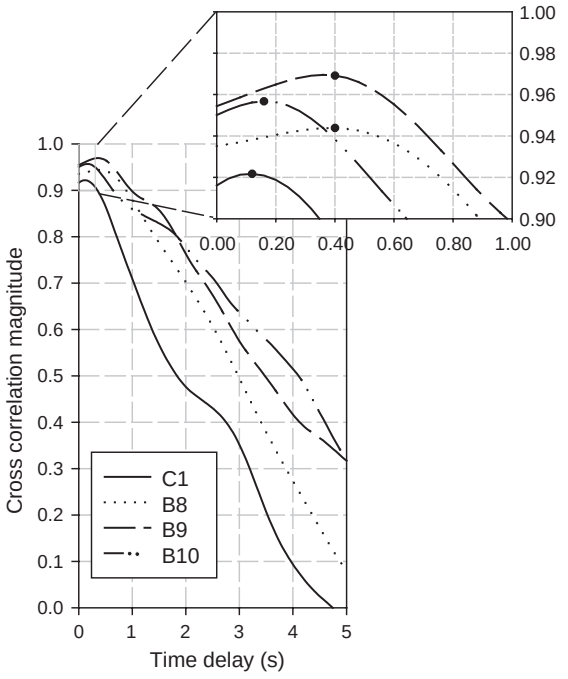

Fig. 8. Cross-correlation between measured swash depth at the still water shoreline and run-up lengths for different experimental cases.

Comparisons of model results to measured values are listed in Table 2. The second column lists the measured maximum run-up length, x_{mm}, of each case while columns 3 and 6 list the calculated maximum run-up lengths, x_{mc}. With the exception of case C1 ($\tan\beta$=0.2), the model without swash interaction over-predicts the maximum run-up length. The largest difference between measured and predicted maximum run-up lengths obtained with the model including swash interaction is 7% for case B10, while the predicted maximum run-up length was more than doubled for the same case when the model without swash interaction was employed.

The overall shape of the shoreline motion, particularly in the beginning stage, is better represented without swash interaction. This is true for all cases with $\tan\beta$=0.07 where the predicted run-up lengths of the first bores are overestimated. This is likely due to some other mechanism not accounted for at the SWS in the simple model presented here. Although the model does not perform better at the initial stages of the shoreline motion, the maximum run-up and overall shape thereafter is well represented. The root-mean-square error (rmse) is a measure of the average absolute difference between observed and calculated values and may be used to asses the accuracy of the model. Smaller rmse values indicate a better fit, and thus suggest that the model performs better with the inclusion of the swash interaction module, particularly for the cases with $\tan\beta$=0.07. For case C1, there is not much improvement when swash interaction is accounted for in the model supporting the notion that swash interaction becomes increasingly important as the foreshore slope decreases.

In all cases except C1, Shield's parameter (Eq. (9)) was less than the critical value 0.8, (Wilson, 1989) for sheet flow so that the clear-fluid friction factor (Eq. (7)) was used, resulting in a value of $0.0050 \le f_u \le 0.0059$ and $0.0053 \le f_b \le 0.0072$ with 2 cm $\le \delta h_u \le$ 4 cm and 1 cm $\le \delta h_b \le$ 3 cm. Simulations for case C1, with the steeper foreshore, resulted in a Shield's parameter in excess of 0.8 for the first two peaks. The sediment-laden friction factor (Eq. (8)) was calculated to be 0.0063 for both up-rush events and 0.0071 and 0.0073 for the back-wash of the first and second waves, respectively (uniform sands were used in the experiment and so the approximation $D_{90} \approx D_{50}$=0.13 mm was made). The calculated friction values are on the lower end of what Puleo and Holland (2001) calculated. There was little sediment transport observed during the experiment, supporting the use of the clear-fluid friction factor for most of the time. It should be noted, however, that the Shield's parameter commonly exceeds 0.8 in field studies and that sheet flow has been observed during much of the swash cycle, predominantly during the up-rush (e.g., Hughes, 1995).

Holland and Puleo (2001) found that the ballistic model gave best results with f_u=0.01 and f_b=0.04 with respect to the minimum overall error between calculated and measured swash trajectories. These constant values were input to the model. Simulation results showed little change of the overall shape of the trajectories and only marginally reduced the maximum run-up length. This was true for both cases with and without swash interaction.

In order to highlight the effect of including swash interaction in the model, predicted excursion lengths of individual bores for case B10 are plotted with solid lines in Fig. 12. The superposition of the parabolas is highlighted with the thicker solid line

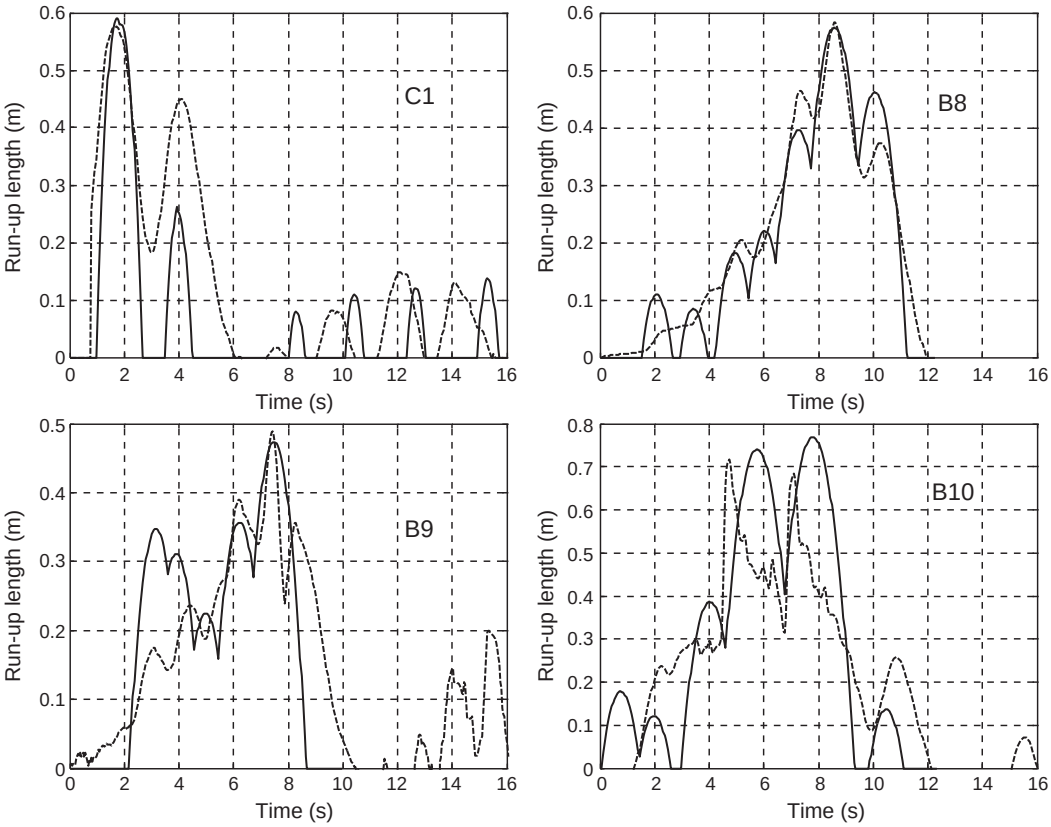

Fig. 9. Measured (dashed lines) and simulated (solid lines) run-up lengths with swash interaction. (N.B. Vertical scale differs between panels).

and is the predicted shoreline motion without swash interaction (Fig. 10). The line marked with ×'s in Fig. 12 depicts the calculated shoreline trajectory when swash interaction is accounted for. Following the trajectory with swash interaction, two collisions on the beach face above the SWS are evident: one where the back-wash of the third parabola marked with ×'s intersects with the up-rush of the fourth solid-lined parabola, and another where the back-wash of the fourth ×-marked parabola intersects with the up-rush of the fifth solid-lined parabola. Following the collisions it can be seen how the back-wash reverses direction to become up-rush but with limited excursion length due to velocity of the back-wash acting against the up-rush.

The effect of the imposed exponentially decaying velocity at the SWS can be seen in the up-rush of the third and last swash-interaction parabolas. Although the back-wash has returned past the SWS, its outgoing velocity is assumed to decay exponentially at the SWS so as to impede the initial velocity of the third and sixth incoming bores (solid lines). The effect can be seen in Fig. 12b showing the same predicted shoreline trajectory with swash interaction in addition to the resulting leading edge velocity. Note the exponential velocity decays after the second, fifth and sixth parabolas return to the SWS. As stated previously, this is a crude estimate to try to account for interaction between outgoing back-wash and incident bores, but without this adjustment, predicted run-up lengths were consistently overestimated.

A look at Fig. 9 shows that accounting for swash interaction has little effect on case C1, which has a steeper foreshore slope ($\tan\beta$=0.20) than the other cases ($\tan\beta$=0.07). The largest difference is for the second wave, as this wave is affected by the exponentially decaying velocity at the SWS of the first wave. In all B cases ($\tan\beta$=0.07), the maximum run-up length is overestimated when the sequential swash interaction is not accounted for.

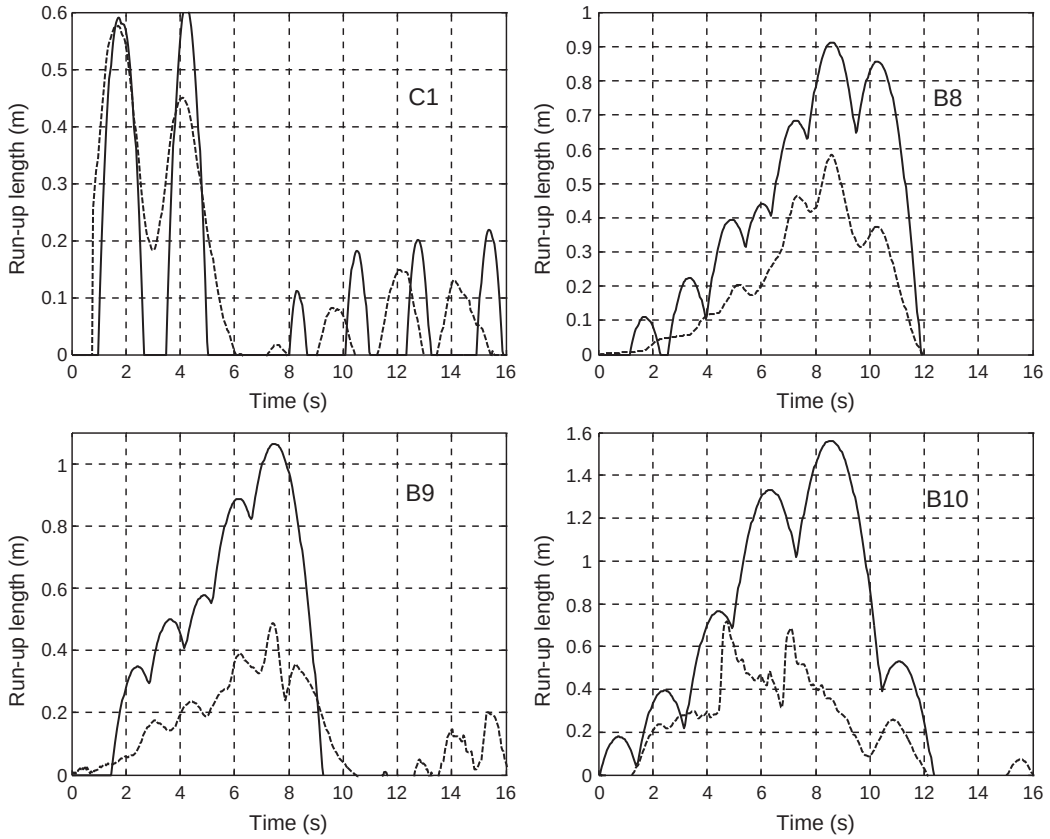

Fig. 10. Measured (dashed lines) and simulated (solid lines) run-up lengths without swash interaction. (N.B. Vertical scale differs between panels).

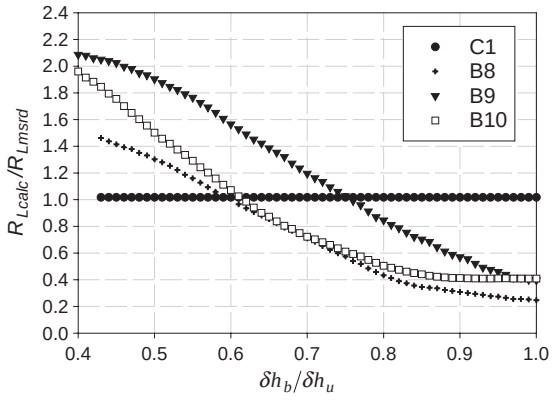

Fig. 11. Sensitivity of run-up length to changes in the relative magnitude of $\delta h_b/\delta h_u$.

The potential for swash interaction can be checked theoretically by comparing Eq. (12) with the incident wave period. Table 3 lists the results using u_0 calculated with measured δh_u and δh_b, maximum wave height at the SWS, and the friction factor, f, calculated with Eq. (7). The total swash duration is nearly twice the incident wave period for the cases with $\tan\beta$=0.07, suggesting a high degree of

Table 2
Comparison of measured and simulated run-up

Case	x_{mm} (m)	With swash interaction			Without swash interaction		
		x_{mc} (m)	% Error	rmse (m)	x_{mc} (m)	% Error	rmse (m)
C1	0.58	0.59	2	0.13	0.61	5	0.12
B8	0.58	0.57	−2	0.05	0.91	57	0.26
B9	0.49	0.48	−2	0.11	1.06	116	0.38
B10	0.72	0.77	7	0.17	1.56	117	0.61

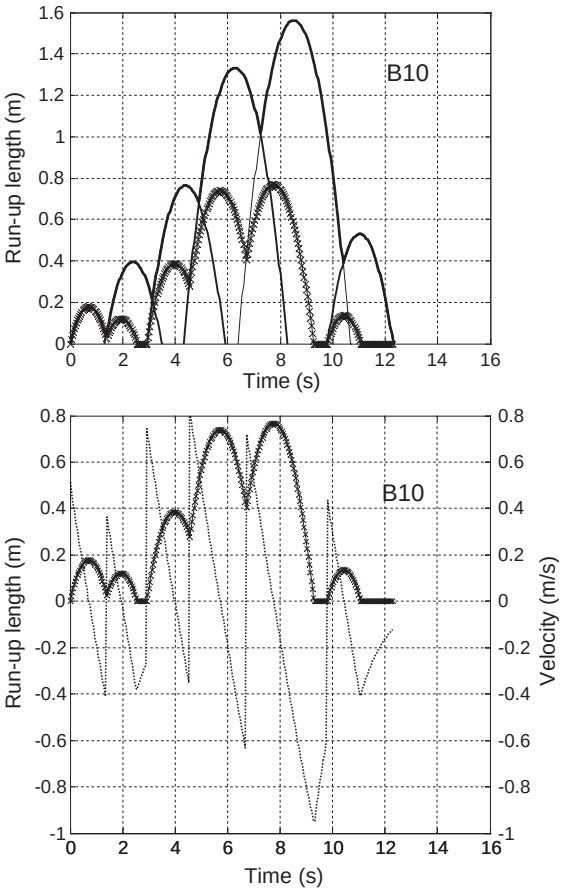

Fig. 12. Comparison of model results for case B10 with (line marked with ×'s) and without (solid line) accounting for swash interaction.

swash interaction. For case C1 with tanβ=0.20, the predicted swash duration is slightly less than the incident wave period suggesting no interaction between subsequent swash waves. This corroborates fairly well with measured results shown in Fig. 6 where it can be seen that there is significant swash interaction for all mild slope cases and some interaction between the first two waves in case C1 with the steeper slope. If friction factors on the order of f_u=0.01 and f_b=0.04 were used, as suggested by Puleo and Holland (2001), then the predicted swash durations would be slightly shorter but still longer than the incident wave periods. The fifth column in Table 3 lists predicted swash durations neglecting friction, T_{sg}. As expected, swash durations without friction are consistently longer than calculated swash durations with friction.

6. Conclusions

Modifications were made to a model that includes the effects of bed friction and describes shoreline displacement as a consequence of bores collapsing at the initial still water shoreline (SWS). Modifications were made to account for interaction between subsequent bores in the swash zone at and above the SWS. Two mechanisms of swash interaction are described: the first is 'catch-up and absorption' where the front of a wave moving landward (up-rush) is passed by a subsequent bore moving in the same direction. The second process is 'collision' whereby two separate fronts collide as the back-wash of a preceding swash lens meets the front of a subsequent swash wave during its up-rush phase. New trajectories of the shoreline are calculated when fronts collide based on the principles of momentum for fluid elements at the leading edges of the colliding swash lenses. The model is a gross simplification of the true process but does appear to at least partially grasp the mechanisms involved with the interaction of subsequent swash waves.

Modifications were also made to account for the effects that outgoing back-wash may have on incident bores at the SWS. This was done by imposing an exponentially decaying velocity of the back-wash following its return past the SWS. Measured swash depths at the SWS were used in the model to calculate initial shoreline velocities as opposed to directly measuring the initial up-rush velocities. Hence, any opposing velocity that the preceding back-wash may have on the collapsing bore would not be accounted for unless the wave height was decreased. Inputs to the model were measured wave heights at the SWS and their arrival times. Leading edge swash heights

Table 3
Calculated swash durations and measured incident wave periods (s)

Case	T_{su}	T_{sb}	T_s	T_{sg}	T
C1	0.81	0.81	1.61	1.67	1.70
B8	1.49	1.47	2.96	3.34	1.30
B9	1.64	1.65	3.29	3.60	1.30
B10	2.00	2.02	4.02	4.36	2.20

were predicted with a previously published empirical equation (Hughes, 1992).

The model was tested with data from a small wave tank experiment conducted for this study. Energy spectra of the swash depth at the SWS indicate that there is significant short wave energy remaining at this point and thus it may be inferred that the model describing shoreline motion as a result of collapsing bores at the SWS is applicable. Wave groups consisting of increasing and subsequently decreasing wave heights and representing idealized vessel generated wave trains were employed in the experiment. Results for four cases, one with a slope of $\tan\beta$=0.20 and three with slope $\tan\beta$=0.07, are presented. Model results show that there is significant improvement in predicting the maximum run-up length if swash interaction is accounted for on the milder slope cases. The largest change in error associated with predicting the maximum run-up length is reduced from 117% to 7% (case B10) and the root-mean-square errors of the entire time series for all three cases are substantially decreased. For the case with $\tan\beta$=0.20 there is no improvement when swash interaction is accounted for.

An equation predicting the duration of the up-rush and back-wash including effects of friction was developed. The equation was applied to the laboratory data for which it was found that the total swash duration (up-rush plus back-wash) was predicted to be much longer than the incident wave period for the cases with milder foreshore slopes ($\tan\beta$=0.07). The longer duration of the swash as compared to incident periods correctly predicts that there would be substantial interaction between subsequent swash waves. The total predicted swash duration for the case with a steeper foreshore ($\tan\beta$=0.20) was slightly less than the incident wave period. This was true for the most part, with the exception of the first two waves of the packet which did meet up within the swash zone.

Acknowledgements

Many thanks to Dr. Steve Hughes, Coastal Hydraulics Laboratory, US Army Engineer Research and Development Center (CHL) for providing the code to generate waves in the laboratory tank, Dr. Nicholas Kraus, CHL for valuable discussions and providing access to the tank, and Dr. Atilla Bayram (presently with Han-Padron Assoc.) who was instrumental to implementing the experiment. Mr. Lasse Johansson at the Swedish Meteorological and Hydrological Institute kindly provided vessel generated wave measurement data. We would also like to thank anonymous reviewers for detailed critiques of the paper. Financial support from the Swedish Research Council and VINNOVA (as part of the project 'The interaction between large and high-speed vessels and the environment in archipelagos') is gratefully acknowledged. Support for the laboratory experiment was provided by the Coastal Inlets Research Program, Inlet Channels and Geomorphology Work Unit.

References

Baldock, T.E., Holmes, P., 1999. Simulation and prediction of swash oscillations on a steep beach. J. Coast. Eng. 36, 219–242.

Baldock, T.E., Holmes, P., Horn, D.P., 1997. Low-frequency swash motion induced by wave grouping. J. Coast. Eng. 32, 197–222.

Cross, R.H., 1967. Tsunami surge forces. J. Waterw. Harb. Div. 93 (WW4), 201–231.

Erikson, L., Hanson, H., 2005. A method to obtain wave tank data using video imagery and how it compares to conventional data collection techniques. J. Comp. Geosci. (in press).

Hibberd, S., Peregrine, D.H., 1979. Surf and run-up on a beach: a uniform bore. J. Fluid Mech. 95, 323–345.

Ho, D.V., Meyer, R.E., Shen, M.C., 1963. Long surf. J. Mar. Res. 21, 219–230.

Holland, K.T., Puleo, J.A., 2001. Variable swash motions associated with foreshore profile change. J. Geophys. Res. 106 (C3), 1623–4613.

Hughes, M., 1992. Application of a non-linear water theory to swash following bore collapse on a sandy beach. J. Coast. Res. 8 (3), 562–578.

Hughes, M., 1995. Friction factors for wave up-rush. J. Coast. Res. 11 (4), 1089–1098.

Hughes, M., Masselink, G., Hanslow, D., Mitchell, D., 1997. Toward a better understanding of swash zone sediment transport. Proc. Coastal Dynamics '97, pp. 804–813.

Irribarren, C.R., Nogales, C., 1949. Protection des ports. Sect. 2, Comm. 4, 17th Int. Nav. Cong., Lisbon, pp. 31–80.

Johansson, L., 2000. Personal communication. Swedish Meteorological and Hydrological Institute.

Kemp, P.H., 1975. Wave asymmetry in the nearshore zone and breaker area. In: Hails, J., Carr, A. (Eds.), Nearshore sediment dynamics and sedimentation. Wiley-Interscience, New York, pp. 47–67.

Kirkgöz, M.S., 1981. A theoretical study of plunging breakers and their run-up. J. Coast. Eng. 5, 353–370.

Mase, H., 1988. Spectral characteristics of random wave run-up. Coast. Eng. 12 (2), 175–189.

Mase, H., 1989. Random wave run-up height on gentle slope. J. Waterw. Port Coast. Ocean Eng. 115 (5), 649–661.

Mase, H., 1994. Up-rush back-rush interaction dominated and long wave dominated swash oscillations. Int. Symp. Waves-Physical and Numerical Modeling Proc. UBC, Vancouver, 316–325.

Mase, H., Iwagaki, Y., 1984. Run-up of random waves on gentle slopes. 19th Coastal Eng. Conf. Proc., ASCE, pp. 593–609.

Miller, R.L., 1968. Experimental determination of run-up of undular and fully developed bores. J. Geophys. Res. 73 (14), 4497–4510.

Puleo, J.A., Holland, K.T., 2001. Estimating swash zone friction coefficients on a sandy beach. J. Coast. Eng. 43, 25–40.

Shen, M.C., Meyer, R., 1963. Climb of a bore on a beach: 3. Run-up. J. Fluid Mech. 16, 113–125.

Svendsen, I.A., Madsen, P.A., 1984. A turbulent bore on a beach. J. Fluid Mech. 148, 79–96.

Van Rijn, L.C., 1982. Equivalent roughness of alluvial beds. J. Hydraul. Div. 108 (HY10), 1215–1218.

Waddell, E., 1973. A field investigation of swash characteristics. Coast. Eng. Jpn. 16, 61–71.

Wilson, K.C., 1988. Frictional behavior of sheet flow. Progress Report 67. Institute of Hydrodynamic and Hydraulic Eng. Tech. Univ. of Denmark, 11–22.

Wilson, K.C., 1989. Friction of wave-induced sheet flow. J. Coast. Eng. 12, 371–379.

Yeh, H.H., Ghazali, A., Marton, I., 1989. Experimental study of bore run-up. J. Fluid Mech. 206, 563–578.